RSC Advances

PAPER

View Article Online
View Journal | View Issue

Cite this: *RSC Adv.*, 2025, **15**, 46506

Eco-friendly synthesis of novel pyrazole derivatives and their anticancer and CDK2 inhibitory activities

Samar A. Abubshait,[ab] Lamia H. T. Amin,[c] Abeer M. El-Naggar,[*d] Mohamed G. Elbanna[d] and Kurls E. Anwer[d]

Received 19th July 2025
Accepted 11th November 2025

DOI: 10.1039/d5ra05212b

rsc.li/rsc-advances

A series of 1-(2-pyridinyl)-4-aryl-1*H*-pyrazole-3,5-diamine derivatives (**2–12**) were designed and synthesized using a one-pot multicomponent reaction *via* both microwave-assisted and conventional techniques. The structural properties of the new compounds were established using spectroscopic data. The new derivatives were biologically assessed as promising CDK2 enzyme inhibitors. Then, the target pyrazoles were screened against both HepG2 and MCF-7 malignant cell lines. Compounds **4**, **7**, and **10** revealed significant CDK2 inhibitory activities with comparable potencies (IC_{50} = 0.75, 0.77 and 0.85 μM, respectively) to that of roscovitine (IC_{50} = 0.99 μM). Additionally, compounds **5**, **6**, and **11** demonstrated the best inhibitory activities, which are twice the activity of roscovitine towards CDK2, with IC_{50} values of 0.56, 0.46, and 0.45 μM, respectively. Concerning the cytotoxic activity, compound **5** displayed potent cytotoxicity (IC_{50} = 13.14 and 8.03 μM) against the HepG2 and MCF-7 cell lines, respectively. Further investigation on the mechanism demonstrated that **5** induced apoptosis, increased the proapoptotic protein Bax level, and reduced the antiapoptotic Bcl-2 level in the cells of MCF-7. Finally, the molecular docking study showed bioactive analogues that fit well in the CDK2 active site *via* various interactions.

1. Introduction

Interestingly, pyrazole derivatives are deemed as one of the most significant heterocyclic derivatives that have broad usage in nano-biotechnology,[1,2] DNA-encoded library technology,[3] pigments, dyes,[4,5] and the petrochemical industry.[6,7] Also, recently, pyrazoles have shown widespread biological and pharmacological activities, such as anticancer,[8–10] antimicrobial,[11,12] anti-phlogistic,[13,14] analgesic,[15] acaricidal,[16] anthelmintic,[17] antiviral,[18] antagonistic,[19] antioxidant,[20–22] herbicidal,[23] antifungal[24] and antibacterial activities.[25,26] Conversely, heterocyclics that contain more than one nitrogen atom have excellent and diverse therapeutic potential and are pivotal in many industrial applications.[27–30]

Green chemistry is the science of designing chemical processes that reduce and or eliminate the hazardous products of reactions. It prevents pollution at a molecular level. Microwave techniques used in the synthesis of heterocyclic compounds are also significant branches of green chemistry methods. The one-pot multicomponent system[31–34] is considered one of the essential techniques for reaction preparation with more facile productivity performance, and it gives highly desired products from simple starting materials and a single run. So, these techniques attract more attention because they are environmentally safe, offer convenient and easy improvements to reaction time and yield, and provide extremely energy-efficient synthetic operations. Comparing both microwave irradiation techniques with the thermally conventional technique, it is clear that the microwave irradiation technique is environmentally friendly, easily controlled, and more ecologically tolerant. As advantages, many reactions of the heterocyclic derivatives are carried out under relatively clean and mild conditions with relatively high yields and short reaction times.[35–37] So, now, this type of green synthesis is considered a very important technique in heterocyclic derivative preparation because of its mild conditions and simplicity. Owing to the above advantages of heterocyclic derivatives and depending on their highly favoured site applications in the industry and biology, more efforts have been put into the preparation of many novel heterocyclic compounds.[38–40]

On the other hand, cancer is a global health problem in which deviant cells in the body divide and proliferate uncontrollably, attacking nearby tissues and in extreme cases, complete biological systems.[41,42] While cell cycle control is mediated *via* governing proteins, which involve kinases that rely on cyclin for their functions (CDKs). CDKs belong to the threonine/serine kinases family that regulates the cell cycle

[a]*Department of Chemistry, College of Science, Imam Abdulrahman Bin Faisal University, P. O. Box 1982, Dammam 31441, Saudi Arabia. E-mail: sabubshait@iau.edu.sa*

[b]*Basic and Applied Scientific Research Centre, Imam Abdulrahman Bin Faisal University, P. O. Box 1982, Dammam 31441, Saudi Arabia*

[c]*Department of Pharmaceutical Medicinal Chemistry and Drug Design, Faculty of Pharmacy (Girls), Al-Azhar University, Nasr City, Cairo, Egypt*

[d]*Chemistry Department, Faculty of Science, Ain Shams University, Abbassia, Cairo, 11566, Egypt. E-mail: kurlsekram@sci.asu.edu.eg*

phases, mostly division, gene transcription, and other post-translational events.[43] For instance, CDK2 has a crucial role in the cell cycle sequence from the G1 to S phase transition, in addition to encouraging the DNA repair system.[44] Therefore, CDK2 enzyme inhibition can lead to cell arrest at both the G2/M and G1/S phases and enhance apoptosis.[45,46] CDK2 is overexpressed in diverse kinds of cancer, such as breast cancer, liver cancer, colorectal carcinoma, pancreatic cancer, melanoma, ovarian carcinoma, lung carcinoma, and osteosarcoma. As a result, the inhibition of CDK2 is thought to be an attractive target for the evolution of novel cytotoxic agents.[47,48] The promising antitumor effect of several CDK inhibitors containing a pyrazole core has been reported in various literature (dinaciclib, roscovitine, olomoucine, purvalanol A and B, CVT313, CYC065, and BS-194), some of which have progressed into clinical investigation.[41,49–51]

Investigating the complex crystal structure of CDK2-roscovitine shows an important interaction between the amino-pyrazolopyrimidine of roscovitine and Leu83 in the hinge region. Roscovitine also interacts with the active site through many hydrophobic interactions; the isopropyl group occupies a hydrophobic pocket. Lastly, the benzyl moiety is pointed out to the solvent-accessible area and has been found to interact with the Lys89 amino acid.[41,50]

In light of published research studies on the design and synthesis of chemotherapeutic agents targeting CDKs, this work is dedicated to synthesizing a series of new pyrazole derivatives (**2–12**) *via* the reaction of 2-hydrazinylpyridine (**1**) with different 2-(aryl-diazenyl)malononitrile derivatives using conventional and microwave methods. The rational design of the new pyrazoles depends on the simplification of the pyrazolopyrimidine scaffold of dinaciclib and the purine ring of roscovitine (Fig. 1). The amino groups in all the prepared compounds are expected to interact with the crucial amino acid (Leu83) in the pivot region. Moreover, the roscovitine benzyl group and the pyridine oxide moiety of dinaciclib are replaced with a substituted phenyl moiety to maintain the compound's active-site interactions. Finally, the hydrophobic isopropyl group of roscovitine and the ethyl group of dinaciclib are replaced by a pyridine moiety in the new desired compounds. All the newly synthesized pyrazole derivatives are investigated as CDK2 inhibitors and antitumour *versus* both mammary breast cancer (MCF-7) and hepatic carcinoma (HCC; HepG2). Furthermore, a docking study of the promising compounds in CDK2 active sites is performed to visualize their relative binding interactions and positions compared with those of roscovitine.

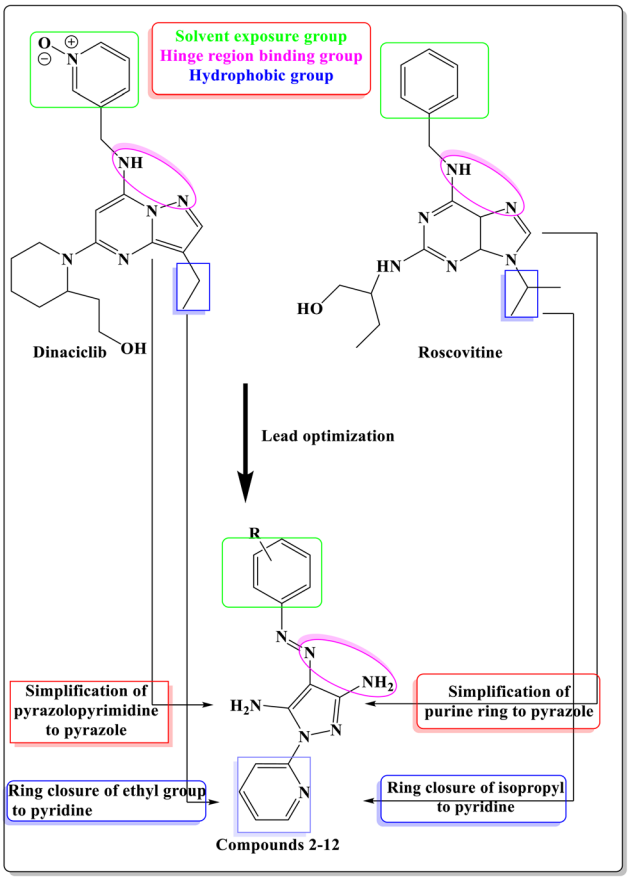

Fig. 1 The rational design of the newly synthesized compounds.

2. Experimental

2.1. Synthesis

The chemicals, reagents, solvents, and starting materials were obtained from Sigma-Aldrich. All solvents used were dried following the chemical's purification handbook for laboratories. To track the reactions and development and control the newly synthesised heterocyclics' homogeneity, TLC was utilized *via* silica gel precoated plates "Merck Kieselgel 60F_{254}, BDH". The melting temperatures of all the newly prepared compounds were determined on the digital Stuart electric equipment (SMP3) for melting points. Microwave irradiation reactions were carried out in an Anton Paar monowave microwave reactor using 10 mL borosilicate glass vials. Infrared absorption spectroscopy (IR, cm^{-1}) was conducted using a PerkinElmer spectrophotometer (model 293) with KBr disks. A Varian Mercury spectrometer (300 MHz) was used for measuring ^1H and ^{13}C-NMR spectra in DMSO-d_6 as a solvent, with tetramethyl silane (TMS) as the reference standard. Multiplicity is symbolized as m for "multiple", t for "triplet", s for "singlet", q for "quartet", d for "doublet", or combinations thereof. Coupling constants (J, Hz) and chemical shifts (δ, ppm) were measured. Mass spectroscopic analysis was carried out using the electron ionization technique on a Shimadzu Gas chromatograph (GC-2010, 70 eV) mass spectrometer. Elemental microanalysis was carried out on a PerkinElmer CHN analyzer (model 2400), and the excellent microanalysis results were within ±0.4% of the theoretical expectations. Different isolated pyrazoles were formed with very interesting structural features.

2.1.1. General preparation method of the 1-(2-pyridinyl)-4-(aryl)-1*H*-pyrazole-3,5-diamine derivatives (2–13). A solution of 2-hydrazinylpyridine (**1**) (0.01 mol, 1.09 mL) in ethanol (20 mL) was refluxed for 2–20 h with each of the following, separately: 2-(3-tolyldiazenyl)malononitrile (0.01 mol, 1.84 g), 2-((4-acetylphenyl)diazenyl)malononitrile (0.01 mol, 2.12 g), 4-

((dicyanomethyl)diazenyl)benzenesulfonic acid (0.01 mol, 2.50 g), 4-((dicyanomethyl)diazenyl)-2-hydroxybenzoic acid (0.01 mol, 2.30 g), *N*-(diaminomethylene)-4-((dicyanomethyl) diazenyl)benzenesulfonamide (0.01 mol, 2.91 g), 2-((4-(phenyldiazenyl)phenyl)diazenyl)malononitrile (0.01 mol, 2.74 g), 2-((2,4,5-trichlorophenyl)diazenyl)malononitrile (0.01 mol, 2.71 g), 2-((3-nitrophenyl)diazenyl)malononitrile (0.01 mol, 2.15 g), 2-((4-methoxyphenyl)diazenyl)malononitrile (0.01 mol, 2.00 g), 2-((dicyanomethyl)diazenyl)benzoic acid (0.01 mol, 2.14 g), 2-((2-chlorophenyl)diazenyl)malononitrile (0.01 mol, 2.04 g) and 2-(thiazol-2-yldiazenyl)malononitrile (0.01 mol, 1.77 g). After the reaction mixture had cooled, the obtained solid substance was separated through filtration, washed four times using ethanol (25 mL), and crystallized using a suitable dissolving agent to give compounds **2–12**, respectively.

*2.1.1.1. 1-(2-Pyridinyl)-4-(3-tolyldiazenyl)-1H-pyrazole-3,5-diamine (**2**).* Orange crystals from ethanol; yield 61%; mp 188–190 °C. IR (cm^{-1}) ν: 3419, 3390, 3313, 3167 ($2NH_2$), 1620 (C=N), 1595 (C=C), 1573 (N=N). ^1H NMR (DMSO-d_6, δ ppm): 2.37 (s, 3H, CH_3), 6.12 (br., 2H, NH_2, D_2O exchangeable), 7.10–7.67 (m, 7H, Ar–H), 7.93 (br., 2H, NH_2, D_2O exchangeable), 8.27–8.42 (s, 1H, Ar–H); ^{13}C NMR (DMSO-d_6, δ ppm): 21.6, 112.3 (2C), 114.6, 118.7 (2C), 119.5, 121.6, 128.6, 129.1, 138.6, 139.7, 147.4, 153.7 and 154.2; anal. calcd for: $C_{15}H_{15}N_7$ (293): C, 61.43; H, 5.12; N, 33.45; found: C, 61.57; H, 5.09; N, 33.34.

*2.1.1.2. 1-(4-((3,5-Diamino-1-(2-pyridinyl)-1H-pyrazol-4-yl) diazenyl)phenyl)ethan-1-one (**3**).* Brown crystals from methanol; yield 65%; mp 264–266 °C. IR (cm^{-1}) ν: 3427, 3357, 3301 ($2NH_2$), 1650 (C=O), 1603 (C=N), 1595 (C=C), 1573 (N=N). ^1H NMR (DMSO-d_6, δ ppm): 2.33 (s, 3H, CH_3), 6.22 (br., 2H, $2NH_2$, D_2O exchangeable), 7.25–8.43 (m, 8H, Ar–H), 9.74 (br., 2H, $2NH_2$, D_2O exchangeable); anal. calcd for: $C_{16}H_{15}N_7O$ (321): C, 59.81; H, 4.67; N, 30.53; found: C, 59.91; H, 4.59; N, 30.44.

*2.1.1.3. 4-((3,5-Diamino-1-(2-pyridinyl)-1H-pyrazol-4-yl) diazenyl)benzenesulfonic acid (**4**).* Black crystals from methanol; yield 62%; mp > 300 °C. IR (cm^{-1}) ν: 3421 (br., OH), 3340, 3313 ($2NH_2$), 3022 (CH aromatic), 1600 (C=N), 1572 (N=N), 1190 (S=O). ^1H NMR (DMSO-d_6, δ ppm): 6.22 (br., 2H, NH_2, D_2O exchangeable), 7.10–7.67 (m, 7H, Ar–H), 7.93 (br., 2H, NH_2, D_2O exchangeable), 8.27–8.42 (m, 1H, Ar–H), 11.25 (s, H, OH, D_2O exchangeable); ^{13}C NMR (DMSO-d_6, δ ppm): 112.3 (2C), 115.0, 119.6 (2C), 120.5, 124.4, 126.8, 139.8, 147.5, 150.0, 153.7, 154.1 and 175.5; anal. calcd for: $C_{14}H_{13}N_7O_3S$ (359): C, 46.80; H, 3.62; N, 27.30; S, 8.91; found: C, 46.68; H, 3.71; N, 27.34; S, 8.85.

*2.1.1.4. 4-((3,5-Diamino-1-(2-pyridinyl)-1H-pyrazol-4-yl) diazenyl)-2-hydroxybenzoic acid (**5**).* Brown crystals from ethanol; yield 61%; mp > 300 °C. IR (cm^{-1}) ν: 3600–2500 (br., OH & $2NH_2$), 1653 (C=O), 1632 (C=N), 1593 (C=C), 1563 (N=N). ^1H NMR (DMSO-d_6, δ ppm): 6.13 (br., 4H, $2NH_2$, D_2O exchangeable), 7.09–8.40 (m, 8H, Ar–H & COOH, D_2O exchangeable), 16.00 (br., H, OH, D_2O exchangeable); ^{13}C NMR (DMSO-d_6, δ ppm): 107.5, 110.8, 112.3, 114.8 (2C), 119.5 (2C), 119.8 (2C), 130.9, 139.7, 147.5, 156.4, 163.6 and 172.5. Anal. calcd for: $C_{15}H_{13}N_7O_3$ (339): C, 53.10; H, 3.83; N, 28.91; found: C, 53.02; H, 3.69; N, 29.01.

*2.1.1.5. 4-((3,5-Diamino-1-(2-pyridinyl)-1H-pyrazol-4-yl)diazenyl)-N-(diaminomethylene)benzenesulfonamide (**6**).* Reddish brown crystals from ethanol; yield 64%; mp 246–248 °C (MeOH); IR (cm^{-1}) ν: 3451, 3429, 3340, 3316, 3168, 3120 ($4NH_2$), 1627 (C=N), 1592, 1568 (C=C), 1551 (N=N), 1262 (SO_2); ^1H NMR (DMSO-d_6, δ ppm); 5.99 (br., 2H, NH_2, D_2O exchangeable), 6.41 (br., 2H, NH_2 exchangeable), 6.73 (br., 4H, $2NH_2$, D_2O exchangeable), 7.22–8.43 (m, 8H, Ar–H); ^{13}C NMR (DMSO-d_6, δ ppm): 112.3 (2C), 115.8, 119.7 (2C), 121.1 (2C), 127.0 (2C), 139.7, 142.7, 147.5, 154.0, 155.5 and 158.6; anal. calcd for: $C_{15}H_{16}N_{10}O_2S$ (400): C, 45.00; H, 4.00; N, 35.00; S, 8.00. Found: C, 45.09; H, 3.95; N, 34.88; S, 8.07.

*2.1.1.6. 4-((4-(Phenyldiazenyl)phenyl)diazenyl)-1-(2-pyridinyl)-1H-pyrazole-3,5-diamine (**7**).* Orange crystals from ethanol; yield 62%; mp 242–245 °C. IR (cm^{-1}) ν: 3423, 3389, 3308, 3190 ($2NH_2$), 1615 (C=N), 1592 (C=C), 1565, 1511 (N=N); ^1H NMR (DMSO-d_6, δ ppm): 6.04 (br., 2H, NH_2, D_2O exchangeable), 6.50 (br., 2H, NH_2, D_2O exchangeable), 7.20–8.45 (m, 13H, Ar–H); ^{13}C NMR (DMSO-d_6, δ ppm): 111.9, 115.9, 119.2 (2C), 121.6 (2C), 122.5 (2C), 123.7 (2C), 129.4 (2C), 131.2 (2C), 139.3, 147.0, 150.4, 152.2, 153.6, 155.5; anal. calcd for: $C_{20}H_{17}N_9$ (383): C, 62.66; H, 4.44; N, 32.90; found: C, 62.77; H, 4.38; N, 32.85.

*2.1.1.7. 1-(2-Pyridinyl)-4-((2,4,5-trichlorophenyl)diazenyl)-1H-pyrazole-3,5-diamine (**8**).* Orange crystals from methanol; yield 63%; mp 222–224 °C. IR (cm^{-1}) ν: 3443, 3408, 3267 ($2NH_2$), 1634, 1601 (C=N), 1592 (C=C), 1558 (N=N); ^1H NMR (DMSO-d_6, δ ppm): 6.21 (br., 2H, NH_2, D_2O exchangeable), 6.64 (br., 2H, NH_2, D_2O exchangeable), 7.24–8.55 (m, 6H, Ar–H); anal. calcd for: $C_{14}H_{10}N_7Cl_3$ (382.5): C, 43.92; H, 2.61; N, 25.62; Cl, 27.85. Found: C, 44.02; H, 2.55; N, 25.71; Cl, 27.72.

*2.1.1.8. 4-((3-Nitrophenyl)diazenyl)-1-(2-pyridinyl)-1H-pyrazole-3,5-diamine (**9**).* Brown crystals from acetic acid; yield 63%; mp 276–278 °C. IR (cm^{-1}) ν: 3423, 3374, 3308 ($2NH_2$), 1622 (C=N), 1589 (C=C), 1568 (N=N); ^1H NMR (DMSO-d_6, δ ppm): 6.04 (br., 2H, NH_2, D_2O exchangeable), 6.51 (br., 2H, NH_2, D_2O exchangeable), 7.18–8.71 (m, 8H, Ar–H); ^{13}C NMR (DMSO-d_6, δ ppm): 112.0 (2C), 119.9, 121.0, 130.1 (2C), 137.3 (2C), 147.1 (2C), 148.9, 153.7, 154.4 (2C); anal. calcd for: $C_{14}H_{12}N_8O_2$ (324): C, 51.85; H, 3.70; N, 34.57; found: C, 51.91; H, 3.64; N, 34.51.

*2.1.1.9. 4-((4-Methoxyphenyl)diazenyl)-1-(2-pyridinyl)-1H-pyrazole-3,5-diamine (**10**).* Brown crystals from ethanol; yield 65%; mp 250–252 °C. IR (cm^{-1}) ν: 3388, 3280, 3207 ($2NH_2$), 1628, 1603 (C=N), 1592 (C=C), 1544 (N=N); ^1H NMR (DMSO-d_6, δ ppm): 3.84 (s, 3H, OCH_3), 6.90–8.84 (m, 8H, Ar–H), 9.46 (br., 2H, NH_2, D_2O exchangeable), 10.63 (br., 2H, NH_2, D_2O exchangeable), 14.49 (br., 1H, OH, D_2O exchangeable); anal. calcd for: $C_{15}H_{15}N_7O$ (309): C, 58.25; H, 4.85; N, 31.72; found: C, 58.16; H, 5.01; N, 31.88.

*2.1.1.10. 4-((2-Chlorophenyl)diazenyl)-1-(2-pyridinyl)-1H-pyrazole-3,5-diamine (**11**).* Brown crystals from ethanol; yield 61%; mp 204–206 °C. IR (cm^{-1}) ν: 3444, 3413, 3300, 3212, 3154, 3112 ($2NH_2$), 1640 (C=N), 1606 (C=C), 1560 (N=N); ^1H NMR (DMSO-d_6, δ ppm): 5.99 (br., 2H, NH_2, D_2O exchangeable), 6.59 (br., 2H, NH_2, D_2O exchangeable), 7.20–8.43 (m, 8H, Ar–H); ^{13}C NMR (DMSO-d_6, δ ppm): 111.8, 116.2, 116.8, 119.3, 120.5, 127.5, 128.1, 129.9, 130.5, 139.2, 139.9, 147.0, 148.6, and 153.5. Anal. calcd for: $C_{14}H_{12}N_7Cl$ (313.5): C, 53.59; H, 3.83; N, 31.26; Cl, 11.32; found: C, 53.47; H, 3.91; N, 31.14; Cl, 11.48.

Table 1 Physical data comparison between the desired derivatives (2–12) under microwave and conventional techniques

	Time "min"		Yield%		YE		OE		RME		
Cpd no.	MW	Conv.	MW	Conv.	MW	Conv.	MW	Conv.	MW	Conv.	AE
2	1	120	92	61	92.00	0.5083	0.7551	0.5006	75.51	50.06	100
3	2	360	91	65	45.50	0.1806	0.7587	0.5419	75.87	54.19	100
4	4	780	95	62	23.75	0.0795	0.8063	0.5262	80.63	52.62	100
5	3	600	92	61	30.67	0.1017	0.7739	0.5131	77.39	51.31	100
6	3	900	92	64	30.67	0.0711	0.7931	0.5517	79.31	55.17	100
7	2	720	93	62	46.50	0.0861	0.7968	0.5312	79.68	53.12	100
8	4	1200	91	63	22.75	0.0525	0.7831	0.5421	78.31	54.21	100
9	3	840	92	63	30.67	0.0750	0.7684	0.5261	76.84	52.61	100
10	2	480	93	65	46.50	0.1354	0.7704	0.5385	77.04	53.85	100
11	3	960	95	61	31.67	0.0635	0.7696	0.4941	76.96	49.41	100
12	3	660	91	62	30.33	0.0939	0.7436	0.5066	74.36	50.66	100

*2.1.1.11. 1-(Pyridin-2-yl)-4-(thiazol-2-yldiazenyl)-1H-pyrazole-3,5-diamine (**12**).* Black crystals from ethanol; yield 62%; mp 258–260 °C. IR (cm^{-1}) ν: 3301, 3180 ($2NH_2$), 1640 (C═N), 1599 (C═C), 1574 (N═N); ^1H NMR (DMSO-d_6, δ ppm): 6.55 (br., 2H, NH_2, D_2O exchangeable), 6.70–6.79 (m, 2H, Ar–H), 6.93 (br., 2H, NH_2, D_2O exchangeable), 7.10–8.56 (m, 4H, Ar–H); anal. calcd for: $C_{11}H_{10}N_8S$ (286): C, 46.15; H, 3.49; N, 39.16; S, 11.20; found: C, 46.09; H, 3.60; N, 39.28; S, 11.03.

2.2. Microwave-promoted synthesis technique

Microwave-assisted synthesis was performed using the same stoichiometric ratios of reactants as in the conventional procedure. The reaction vial was irradiated at 120 °C under 2–5 bar pressure and 200–400 W power for 1–4 min (Table 1) with constant magnetic stirring. The completion of the reaction was confirmed by TLC. The resulting product was then purified by ethanol washing, followed by recrystallization using a suitable solvent.

2.3. Biological assessment

2.3.1. *In vitro* cyclin-dependent kinase CDK2 inhibitory activity. The inhibitory efficiency of the CDK2 enzyme of our investigated pyrazoles was estimated using Bioscience CDK kits, CDK2 (Catalog #79599), following the manufacturer's instructions.

2.3.2. *In vitro* anticancer properties. The newly synthesized pyrazoles' anticancer effect was evaluated *in vitro* utilizing two different cancer cell lines, including MCF-7 and HepG2. The used cell lines were purchased from ATCC (Rockville, MD). The colorimetric assay aims to convert the yellow color of the tetrazolium bromide (MTT) into purple through formazan formation in viable cells *via* mitochondrial enzyme succinate dehydrogenase (SDH). The first step was culturing the cell lines using 10% FBS in RPMI-1640 medium. Streptomycin and penicillin were supplied as antibiotics, and the cell lines under 5% CO_2 at 37 °C were plated in a 96-well microplate. Following the treatment with changing concentrations of the prepared pyrazoles, cells were cultured at 37 °C for 48 h. Under dark conditions, the cells were maintained during incubation with an MTT reagent at 37 °C for 4 h. The obtained purple-colored products in each well were dissolved in DMSO. The colorimetric assay was conducted using a plate reader at 570 nm, and the result was recorded. The nonlinear regression fitting model was used to calculate the percentage of the relative cell viability (Prism version 8.0, GraphPad). The data were recorded from the means of three separate experiments.[52,53]

2.3.3. Cell cycle analysis. Breast adenocarcinoma cells (MCF-7) were treated with derivative **5** for 48 h at its IC_{50}. Then, the cells furnished by trypsinization were washed twice in PBS and set at 4 °C in ice/ethanol (60%, w/w) for 12 h. After that, the cells were re-washed in PBS, and the ethanol was removed. Later, the cells were stained in a buffer solution containing RNase and propidium iodide (PI, 500 μL) and incubated for 30 min. Finally, a flow cytometer was utilized for cell cycle phase analysis.[54,55]

2.3.4. Apoptotic assay. MCF-7 cell lines were treated using IC_{50} of analogue **5** for 48 h and then trypsinized and subjected to PBS for washing. Thereafter, the cells were stained in a buffer containing 10 μL of V-fluorescein isothiocyanate and 5 μL of propidium iodide (staining solution) at r.t. in a dark place, based on the manufacturer's directions. After dyeing, the cell lines were analyzed using the FACScan analysis flow cytometer.[56]

2.3.4.1. Apoptotic marker (Bcl-2) determination. The enzyme-linked immunosorbent Bcl-2 ELISA detecting kit from Zymed (Catalog #99-0042) was utilized for the quantitative assay of Bcl-2 in human cells following the manufacturer's instructions.

2.3.4.2. Apoptotic marker (Bax) determination. Human active Bax content was determined using the ELISA kit for detecting Human Bax (EIA-4487) based on the manufacturer's guidelines.

2.3.5. Molecular docking simulation study. The molecular docking investigation was achieved using Vina Autodock. The crystal structure information of CDK2 in complex with the ligand roscovitine was obtained from the protein databank (ID code 2A4L). The receptor and the ligand were adapted in the format of pdbqt to carry out the docking procedure using Vina Autodock. M.G.L. systems were utilized to measure the grid layout box features and binding site coordinates. The freely accessible BIOVIA Discovery Studio 2021 visualizer was employed to visualize the predicted 3D and 2D binding modes for the investigated compounds.

2.3.6. Computational study of ADME aspect prediction. ChemDraw 14.0 was used to transform the pyrazole structures into a SMILES dataset. After that, the obtained SMILES were inserted into the freely available SwissADME website to estimate the pharmacokinetic properties, physicochemical aspects, ADME parameters, and/or drug-likeness characteristics of the screened compounds.[57]

3. Results, interpretation, and discussion

3.1. Chemistry and hetero synthesis

The novel pyrazole analogues were synthesized through the reaction sequences clarified in Schemes 1–3. The interesting pharmacological properties of the bifunctional starting 2-hydrazinopyridine (**1**), such as anticancer,[58,59] antibacterial,[60,61] antifungal,[62,63] and anti-inflammatory[64] activities, led us to synthesize a new series of pyrazole derivatives (**2–13**).

Therefore, the reaction of compound **1** with di-nitrogen electrophiles such as 2-(3-tolyldiazenyl)malononitrile, 2-((4-acetylphenyl)diazenyl)malononitrile, 4-((dicyanomethyl)diazenyl)benzenesulfonic acid, 4-((dicyanomethyl)diazenyl)-2-hydroxybenzoic acid, *N*-(diaminomethylene)-4-((dicyanomethyl)diazenyl)benzenesulfonamide, 2-((4-(phenyldiazenyl)phenyl)diazenyl)malononitrile, 2-((2,4,5-trichlorophenyl)diazenyl)malononitrile, 2-((3-nitrophenyl)diazenyl)malononitrile, 2-((4-methoxyphenyl)diazenyl)malononitrile, 2-((dicyanomethyl)diazenyl)benzoic acid, 2-((2-

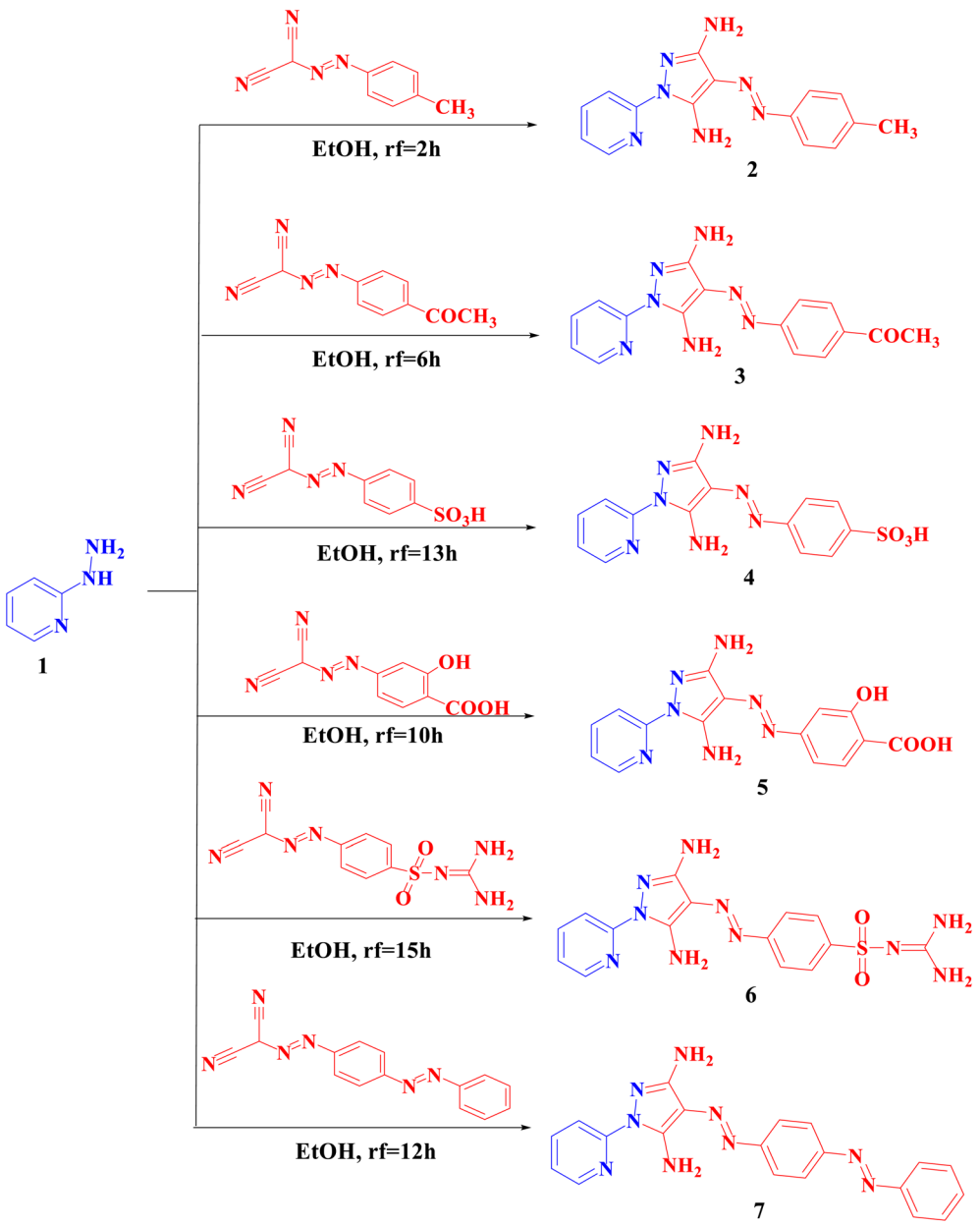

Scheme 1 Preparation of the targeted pyrazole derivatives 2–7.

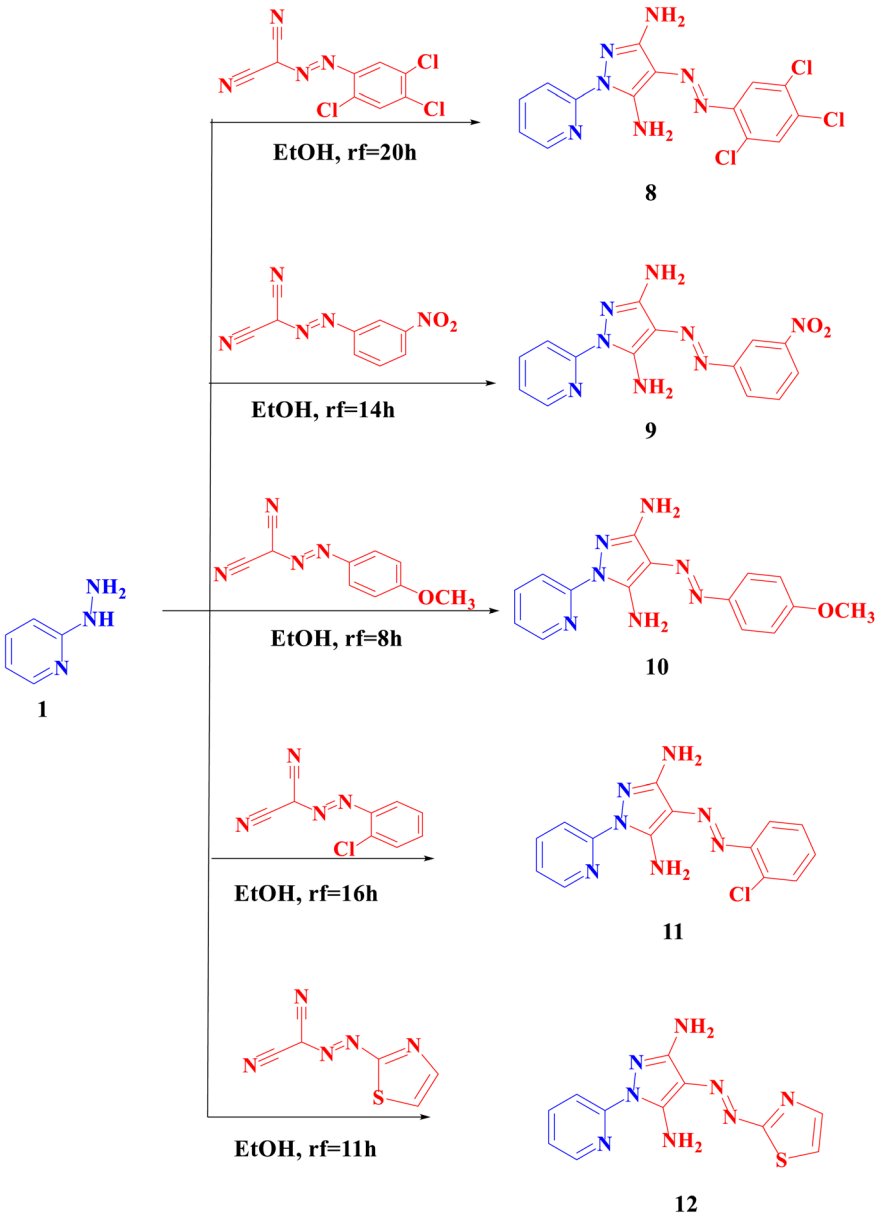

Scheme 2 Preparation of the targeted pyrazole derivatives 8–12.

chlorophenyl)diazenyl)malononitrile and 2-(thiazol-2-yldiazenyl)malononitrile was investigated. The corresponding condensed derivatives (**2–12**) (Schemes 1 and 2) were produced *via* the hydrazine NH_2 group nucleophilic addition on the CN group of the malononitrile derivative, followed by the second addition of the NH group on the second cyano group, which was predicted to yield some interesting biological characteristics (Scheme 3).

3.2. A comparison between microwave and conventional procedures

The synthesis of the series of pyrazoles was performed under conventional and microwave-assisted methods.[65–71] TLC was employed to monitor the reaction process using the two techniques. Table 1 shows that despite the molar concentrations of all reactants in the three disciplines being equivalent, the product yields and reaction times were completely different. The most suitable method for a definite reaction was determined by calculating the yield economy (YE) according to the following equation.

$$\mathrm{YE} = \frac{\text{yield percentage}}{\text{reaction time “min”}}.$$

Moreover, reaction mass efficiency (RME) is a beneficial parameter for the detection of the reaction efficiency, and it is calculated through the following equation.

$$\mathrm{RME} = \frac{\text{products weight}}{\text{reactants weight}}.$$

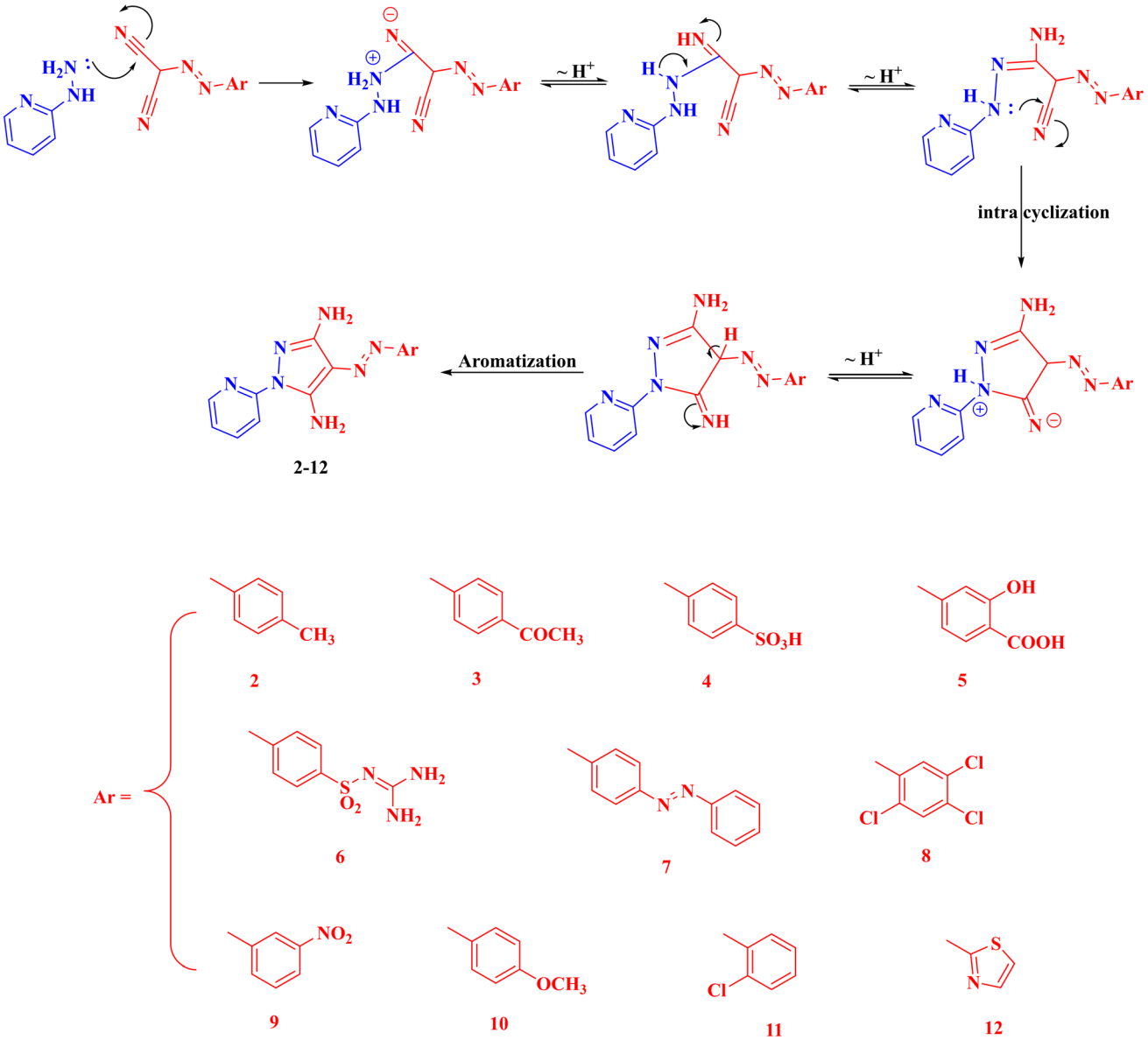

Scheme 3 Preparation mechanism of the pyrazole derivatives 2–12.

The last parameter utilized in the differentiation between the green techniques (grinding and microwave) and the conventional method is the optimum efficiency (OE), which is determined *via* the following equation: $\mathrm{OE} = \frac{\mathrm{RME}}{\mathrm{AE}} \times 10$. (AE) refers to the atomic economy. Such parameters were applied to distinguish the efficacy of the three techniques in the preparation of an identical desired compound. It is to be mentioned that while the other parameters are greater in the microwave, followed by grinding technique and then conventional heating, the AE is the same in all methodologies utilized to synthesize the same compound.

In the microwave technique, the same reactant amount used in conventional reactions was used without a solvent. The TLC was used to monitor the completion of the reaction. The solids formed were washed with ethanol three times and recrystallized

Table 2 CDK2 inhibitory activities of our tested compounds *versus* roscovitine

Comp. ID	IC_{50} (μM) CDK-2
2	1.05 ± 0.2
3	1.2 ± 0.15
4	0.75 ± 0.05
5	0.56 ± 0.03
6	0.46 ± 0.02
7	0.77 ± 0.05
8	1.46 ± 0.5
9	1.5 ± 0.7
10	0.85 ± 0.05
11	0.45 ± 0.02
12	1.24 ± 0.85
Roscovitine	**0.99 ± 0.08**

Table 3 IC_{50} (μM) of the tested compounds against human tumour cells (HepG2 and MCF-7) compared with that of doxorubicin

	IC_{50}	
Comp. ID	HepG2	MCF-7
4	53.84 ± 3.2	48.70 ± 2.8
5	13.14 ± 1.1	8.03 ± 0.6
6	22.76 ± 1.5	26.08 ± 1.7
7	67.12 ± 3.5	35.11 ± 2.2
10	41.59 ± 2.4	15.38 ± 1.2
11	74.18 ± 3.8	61.76 ± 3.4
DOX	**4.50 ± 0.2**	**4.17 ± 0.2**

using the proper solvent. Microwave irradiation was carried out using an Anton Paar monowave 300 with 10 mL borosilicate glass vials for 1–4 min. The conventional thermal reactions were carried out in a porcelain mortar with a pestle for 2–20 h. The obtained products of the same reaction using the three techniques were identical in mp, mixed mp, and TLC. The comparison between the reaction time and yield of the prepared compounds by the two techniques was reported. The microwave reactions afforded higher yields with the lowest times than the conventional reactions. The microwave technique is considered a green method in heterocyclic synthesis. Thus, the microwave technique is better than the conventional techniques.

Table 4 Results of the cell cycle analysis on the MCF-7 cells expressed by (%) of cells in each phase when treated with compound **5**

Compound	% G1	% S	% G2
5/MCF-7	11.98	41.02	47.00
Control/MCF-7	38.02	35.52	26.46

3.3. *In vitro* CDK2 inhibition

The investigated compounds were evaluated for their CDK2 inhibition activity to explore their action mechanism. A reference drug used for comparison was roscovitine, which is regarded as a highly competitive CDK2 ATP inhibitor. The results are reported in Table 2 as the 50% inhibition concentration value of CDK2 (IC_{50}). The enzyme assay results revealed that the tested compounds displayed moderate to potent inhibitory activities at sub-micromolar to low micromolar levels (IC_{50} values of 0.45–1.5 μM).

Compounds **5**, **6** and **11** demonstrated a significant inhibitory effect towards CDK2 and afforded IC_{50} = 0.56, 0.46, and 0.45 μM, respectively. They revealed 2-fold the activity of roscovitine (IC_{50} = 0.99 μM). However, compounds **4**, **7**, and **10** revealed comparable potency of roscovitine against CDK2 (IC_{50} values of 0.75, 0.77 and 0.85 μM, respectively).

3.4. *In vitro* anticancer evaluation

The anticancer activities of the compounds (**4**, **5**, **6**, **7**, **10**, and **11**) showing the most potent inhibitory effect on CDK2 were examined towards two human tumour cell lines, specifically hepatic (HepG2) and breast (MCF-7) carcinoma. The screened compounds' biological activities were measured by the MTT evaluation method. The IC_{50} values were estimated compared with those of the standard drug, doxorubicin, which displayed IC_{50} values of 4.50 and 4.17 μM for the two tested cell lines, respectively.

Derivative **5** displayed potent cytotoxicity (IC_{50} = 13.14 and 8.03 μM), while derivative **6** showed good potency (IC_{50} = 22.76 and 26.08 μM) against the HepG2 and MCF-7 cell lines, respectively. Moreover, pyrazole derivative **10** revealed the third-best activity, compared with doxorubicin, (IC_{50} = 15.38 μM)

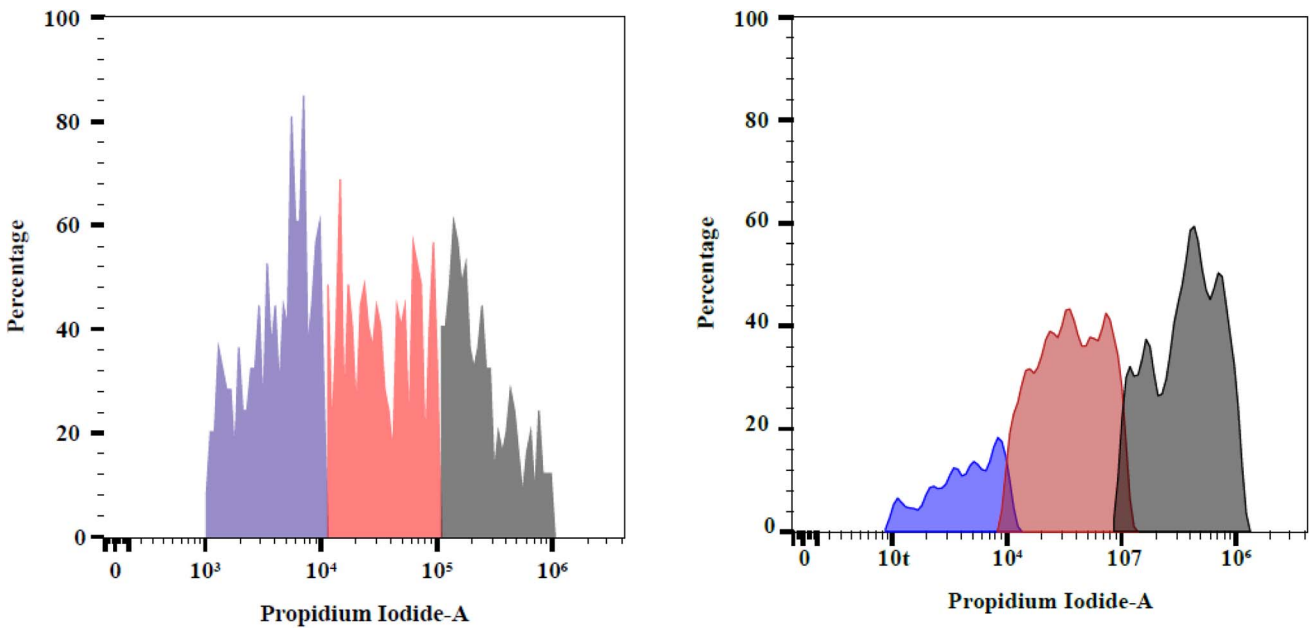

Fig. 2 Cell cycle analysis of the control (on the left side) and compound **5** (on the right side) on the MCF-7 cells.

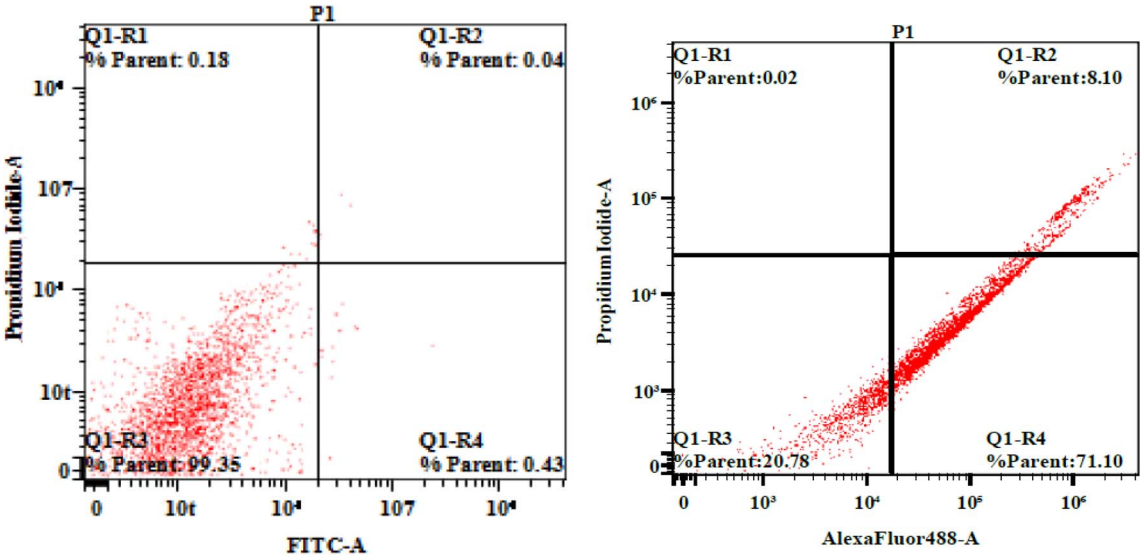

Fig. 3 Effect of the control (the left side) and compound 5 (the right side) on the apoptosis of MCF-7.

Table 5 The effect of compound 5 on the apoptosis/necrosis of the MCF-7 cells

Compound	Total	Early apoptosis	Late apoptosis	Necrosis
5/MCF-7	79.22	71.1	8.10	0.02
Control/MCF-7	0.65	0.43	0.04	0.18

Table 6 Effect of compound 5 on the Bax and Bcl-2 levels

	Bax		Bcl-2	
Comp.	pg mL^{-1}	FLD	ng mL^{-1}	FLD
5	369.15 ± 0.7	6.45	1.72 ± 0.08	0.3
Control	57.22 ± 0.9	1	5.31 ± 0.5	1

against the MCF-7 cell line. Finally, the other synthesized pyrazoles possessed moderate or weak anticancer activities. The results are tabulated in Table 3.

3.5. Cell cycle analysis

The analysis of the cell cycle was conducted to explore the possible underlying antiproliferative mechanism behind the most potent compound. Among the cancer cell lines under evaluation, MCF-7 exhibited the highest sensitivity towards our compounds. So, this work aims to evaluate the effect of pyrazole derivative 5 on the MCF-7 cell cycle. Concerning the compound 5 effect on the cell cycle, the data demonstrated a cell cycle arrest at the S phase from 35.52% to 41.02% and the G2 phase from 26.46% to 47% compared with the control. Further, a decrease in the cell population at the G1 phase, from 38.02% to 11.98%, was observed (Table 4 and Fig. 2). These results indicated that our tested compound showed a 1.8- and 1.2-fold increase in the G2 and S phases, respectively, in comparison to the control cancer cells.

3.6. Apoptosis study

Apoptosis is a planned death process for damaged cells that occurs under physiological and pathological conditions. The

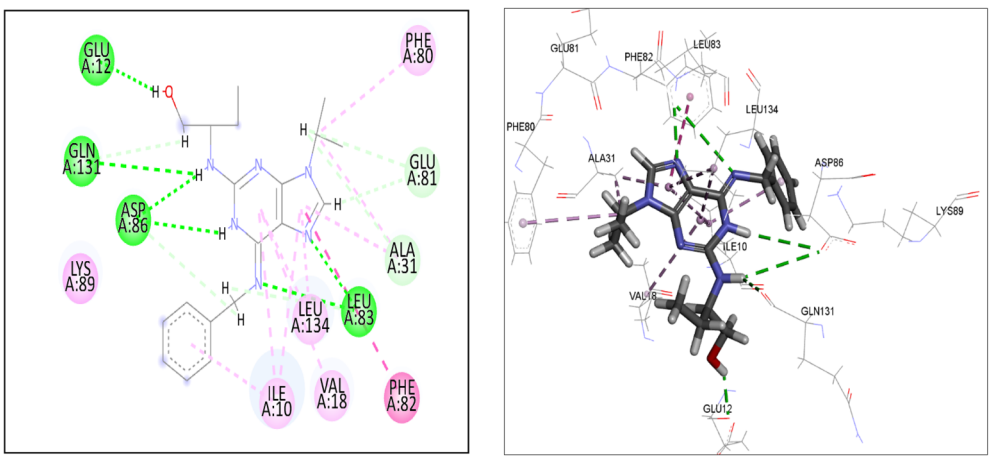

Fig. 4 The proposed 2D (left) and 3D (right) binding modes of roscovitine into the CDK2 active site.

Table 7 The proposed docking scores and interaction of roscovitine and the desired pyrazole derivatives (**5** and **6**)

Comp. no.	Energy score (kcal mol^{-1})	Interaction types (amino-acid residues)	Bond length (Å)
Roscovitine	−7.94	H-bond (Leu83)	2.5
		H-bond (Leu83)	4.2
		H-bond (Asp86)	3.85
		H-bond (Asp86)	4.00
		H-bond (Glu12)	2.11
		H-bond (Gln131)	3.51
		C–H-bond (Leu83)	3.25
		C–H-bond (Asp86)	3.65
		C–H-bond (Glu81)	2.45
		C–H-bond (Glu81)	3.63
		C–H-bond (Gln131)	4.44
		C–H-bond (Ala31)	4.50
		Hydrophobic-π–alkyl (Phe80)	4.66
		Hydrophobic-π–alkyl (Ala31)	3.94
		Hydrophobic-π–alkyl (Ile10)	4.70
		Hydrophobic-π–alkyl (Ile10)	5.14
		Hydrophobic-π–alkyl (Val18)	5.29
		Hydrophobic-π–alkyl (Leu134)	4.29
		Hydrophobic-π–alkyl (Leu134)	4.53
		Hydrophobic-π–alkyl (Ala31)	3.89
		Hydrophobic-π–alkyl (Ile10)	4.23
		Hydrophobic-π–π (Phe82)	5.83
5	−7.40	H-bond (Leu83)	2.26
		H-bond (Leu83)	3.46
		H-bond (Leu83)	4.16
		H-bond (Lys20)	4.34
		H-bond (Asp86)	4.74
		H-bond (Asp86)	2.69
		H-bond (Asp86)	2.80
		H-bond (Gln131)	4.20
		H-bond (Glu81)	4.24
		H-bond (His84)	2.71
		H-bond (Glu8)	1.95
		C–H-bond (His84)	4.59
		C–H-bond (Ala31)	3.98
		C–H-bond (Glu81)	3.69
		Hydrophobic-π–alkyl (Ile10)	4.50
		Hydrophobic-π–alkyl (Ile10)	4.87
		Hydrophobic-π–alkyl (Leu134)	3.98
		π–anion (Glu8)	4.42
6	−6.88	H-bond (Leu83)	2.00
		H-bond (Leu83)	4.26
		H-bond (Lys20)	3.25
		H-bond (Lys20)	2.09
		H-bond (Lys89)	2.67
		H-bond (His84)	3.19
		H-bond (Ile10)	2.72
		H-bond (Leu298)	2.31
		H-bond (Glu8)	2.26
		C–H-bond (Lys89)	4.28
		C–H-bond (Lys20)	4.33
		C–H-bond (His84)	2.53
		C–H-bond (His84)	4.25
		C–H-bond (Glu12)	4.68
		π–alkyl (Ile10)	4.51
		π–anion (Asp86)	3.80
		π–anion (Asp86)	3.69
		π–π (His84)	5.98
		π–cation (Lys89)	2.49
		Hydrophobic amide–π (Gln85)	5.03

disturbance or misguided monitoring of different apoptotic routes results in the out-of-control multiplication of malignant cells.[72,73]

An annexin V binding assay was carried out to study the apoptosis-inducing potential of compound **5**. The apoptotic nature of compound **5** against the MCF-7 cells was measured through flow cytometry detection with propidium iodide (PI) and annexin V-FITC double staining.

The results demonstrated that pyrazole derivative **5** elevated the early ratio of apoptosis from 0.43% to 71.1% and the late ratio of apoptosis from 0.04% to 8.10%. Compound **5** decreased the necrotic cell death from 0.18% to 0.02%, relative to untreated MCF-7 as a control. These data suggested that compound **5** induced programmed cell death *via* apoptosis instead of the necrotic pathway (Fig. 3 and Table 5).

The quadrants in the cytograms represent the following: necrotic cells (higher left quadrant of the cytogram); late apoptotic cells (higher right quadrant of the cytogram); non-apoptotic and non-necrotic cells (living cells) (lower left quadrant of the cytogram); early apoptotic cells (lower right quadrant of the cytogram).

3.7. The influence on mitochondrial apoptotic proteins (Bax & Bcl-2)

The family of the Bcl-2 protein shows a critical contribution in mitochondrial apoptosis control. Among them, Bcl-2 and Bax regulate this process properly; Bcl-2 suppresses it (anti-apoptotic), while Bax induces it (pro-apoptotic).[74] Therefore, achieving an optimal equilibrium between these two proteins is essential for determining the ability of the cells to pass through apoptosis.[75]

During this study, the treatment of MCF-7 *via* the most active derivative (**5**) was performed, and its influence on the Bcl-2 and Bax levels is illustrated in Table 6.

The results revealed that compound **5** raised the Bax protein level by 6.4-fold and decreased the anti-apoptotic Bcl-2 level by 3-fold in comparison with the control. The important parameter is the two-protein ratio. Therefore, the Bax/Bcl-2 ratio of compound **5** was calculated to be approximately 20-fold in comparison with the control, indicating that this compound shifted the cells to undergo apoptosis.

3.8. Docking study

In this study, Autodock Vina software was used to carry out the reference docking simulation study, and the two promising derivatives (**5** and **6**) were docked into the CDK2 enzyme ATP binding site. The interaction and binding affinity of the desired pyrazoles were studied to clarify the biological outcomes, as well as to shed light on the binding poses and interactions. The CDK2 X-ray crystal structure in complex with roscovitine was downloaded from the protein data bank (code 2A4L).[76] The docking procedure was confirmed by re-docking roscovitine inside the CDK2 active site. After that, the RMS deviation was measured (0.99 Å), implying that the used docking procedure obtained an accurate pose orientation. The affinity mode of roscovitine showed that the amino pyrazolopyrimidine moiety was linked to the critical amino acid (Leu83) residue in the hinge region by two hydrogen bonds, in addition to its ability to form three hydrogen bonds, two of them with Asp86 and the last one with Gln131. The benzyl moiety formed a non-conventional hydrogen bond with Asp86. Moreover, the isopropyl group was able to interact with Glu81 and Ala31 through carbon–hydrogen bonds. Besides, the hydroxyl group formed an H-bond with Glu12. Furthermore, the interactions of different hydrophobic natures were recorded with Val18, Lys89, Leu134, Phe80, Phe82, and Ile10 (Fig. 4).

The exploration of the compounds **5** and **6** binding modes exhibited good fitting in the CDK2 active site with energy scores of −7.40 and −6.88 kcal mol^{-1}, respectively. Both compounds established a complex with the ATP binding site that was stabilized by H bonds in the hinge region, together with many hydrophobic connections with the enzyme hydrophobic pocket (Table 7, Fig. 5 and 6).

A similar direction was noticed for both derivatives into the enzyme active pocket, in which the diamino-4-diazenyl pyrazole moiety formed 2 H-bonds with the vital Leu83 amino acid. The NH_2 group at the 3-position formed three H-bonds with Asp86 and Gln131, while the amino group at the 5-position formed an

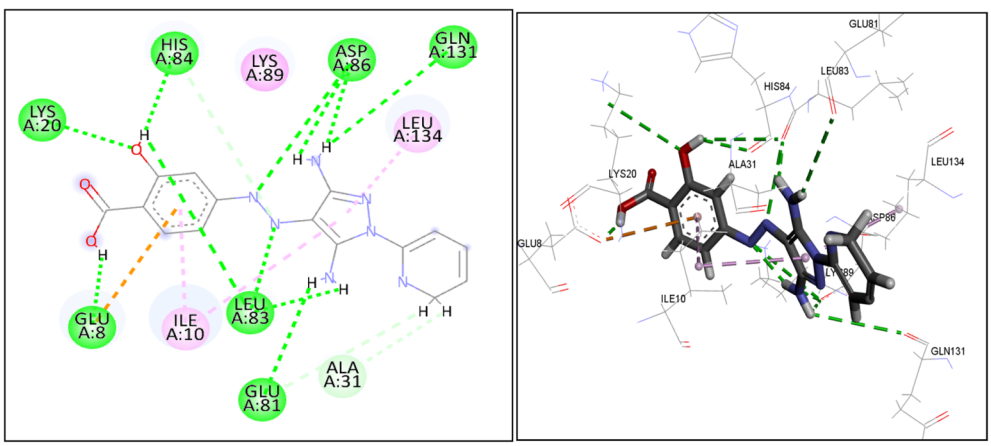

Fig. 5 The proposed 2D (left) and 3D (right) binding modes of **5** into the CDK2 active site.

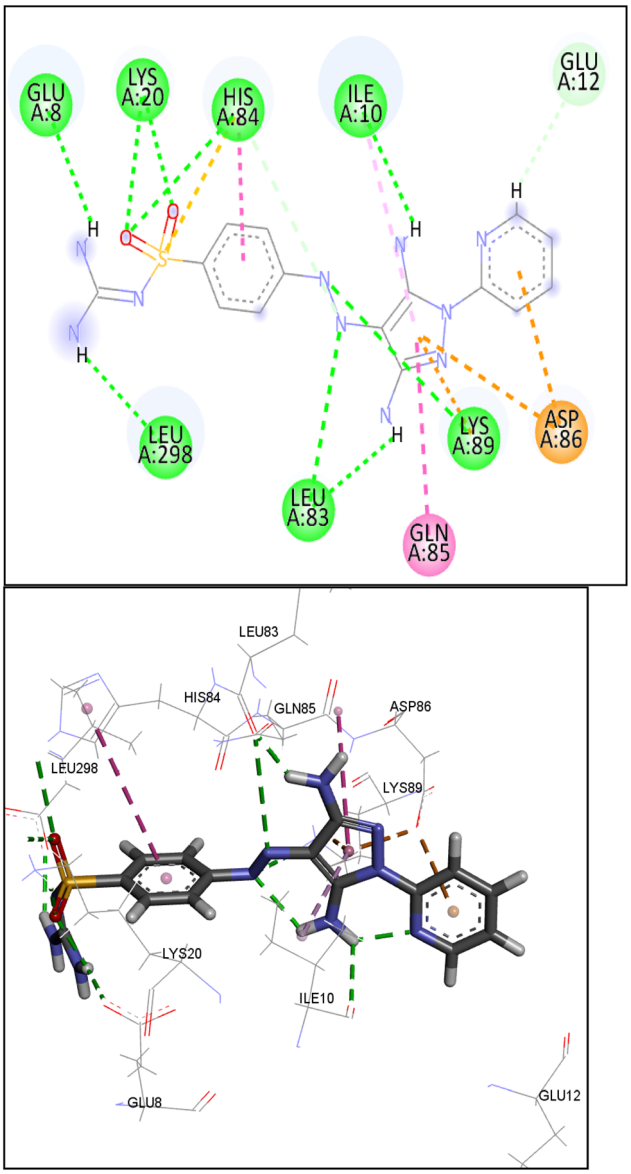

Fig. 6 The proposed 2D (left) and 3D (right) binding modes of **6** into the CDK2 active site.

H-bond with Glu81 in compound **5**. The pyrazole ring was involved in a non-polar interaction with the Leu134 amino acid. The hydroxyl group interacted through three H-bonds with His84, Lys20, and Leu83. The carboxylic group formed an H-bond with Glu8. The phenyl ring could lie well in the hydrophobic pocket of ATP through nonpolar interactions with amino acid Ile10. However, a pi–cation connection was formed between the phenyl ring and Glu8. Concerning compound **6**, the amino group at the 5-position was involved in an H-bond interaction with Ile10, and the pyrazole core formed hydrophobic interactions with Ile10 and Gln85. Diamino methylene-benzenesulfonamide formed five H-bonds with His84, Lys20, Leu298, and Glu8. The benzenesulfonamide ring could fit in the ATP nonpolar pocket, forming a pi–pi interaction with His84 amino acid. Finally, the pyridine moiety formed a carbon–

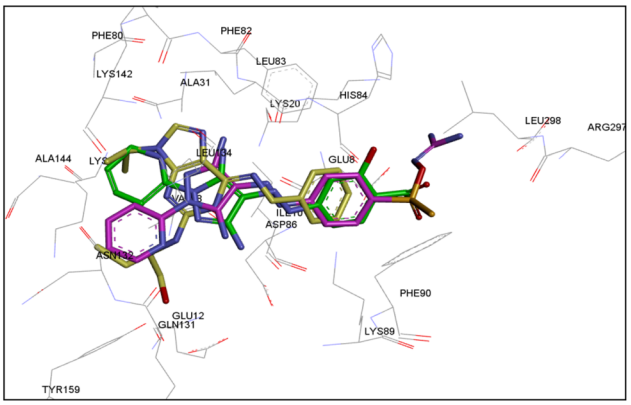

Fig. 7 Superimposition of roscovitine and active compounds **5** and **6**.

hydrogen bond with Glu12 and a pi–anion interaction with Asp86. Thus, we can conclude that the simplification of the fused heterocyclic ring to pyrazole has a positive impact on the activity, as the diamino pyrazole ring could accommodate well and form connections with the same essential amino acids: Leu83, Asp86, Ile10, and Glu81. Moreover, the cyclization of the isopropyl group of roscovitine to pyridine in compound **5** could adapt the hydrophobic pocket and interact with similar amino acids (Ala31 and Glu81) as the isopropyl of the ligand. The overlay of the ligand, roscovitine, with our newly prepared derivatives (**5** and **6**) is presented in Fig. 7.

3.9. *In silico* ADME prediction

According to Lipinski's rule for oral drugs, the permeation or absorption of a heterocyclic molecule is probable when the weight of the molecule is under 500 g mol^{-1}, the calculated value of the octanol–water partition coefficient is lower than **5**, and the molecule possesses not more than five H-bond donors and not more than 10 H-bond acceptors.[77] However, drug-likeness constraints according to Veber's rule were defined as total rotatable bonds $\leq$ 10 and area occupied by polar surface (PSA) $\leq$ 140.[78]

The pharmacokinetic properties of the promising derivatives (**5** and **6**) were predicted *via* the SwissADME online tool. The results revealed that compound **5** had zero Lipinski violations. Concerning Veber's rule, the tested compounds had rotatable bonds between 4 and 5, indicating molecular flexibility to their biotarget, and both compounds had one deviation from Veber rules (TPSA > 140) (Table 8).

Considering the medicinal chemistry and pharmacokinetic parameters of the desired compounds (Table 9), both tested pyrazole derivatives had low gastrointestinal tract absorption and were unable to penetrate the blood–brain barrier. This confirms that the targeted molecules work systemically with no side effects on the CNS.

Furthermore, both studied derivatives have no activities on cytochrome P450 isomers "CYP3A2 and CYP2D6", and consequently, they are expected to have no drug–drug interaction on administration (Table 9).

Table 8 Physicochemical characteristics based on Veber's and Lipinski's rules of compounds 5 and 6

Cpd no.	HBD	HBA	M log *P*	MW	No. of rot. bonds	TPSA	Lipinski's violations	Veber's violations
5	4	7	0.28	339.31	4	165	0	1 TPSA > 140
6	4	7	0.65	400.42	5	214.39	1	1 TPSA > 140

Table 9 Pharmacokinetic properties and medicinal chemistry parameters of tested compounds 5 and 6

Cpd no.	GI absorption	BBB permeation	P-gp substrate	CYP2D6	CYP3A4	Synthetic accessibility
5	Low	No	Yes	No	No	3.03
6	Low	No	Yes	No	No	3.51

SwissADME chemical synthesis Accessibility Score (SA) assumed that the ease of the synthesis was correlated with the molecular fragment's frequency in the obtained molecules. The score ranged from very easy (1) to very difficult (10) to synthesize.[79] Both tested analogues' SA scores were 3.03 and 3.51, suggesting that both could be synthesized on a large scale.

4. Conclusion

In conclusion, novel azo-pyrazole moieties were designed, synthesized *via* two techniques, and evaluated for their potential CDK2-enzyme inhibition effects. The anticancer activity of the most active analogues in the enzyme inhibitory studies was assessed against two different human cancer cell lines, in comparison to doxorubicin. Compound **5** exhibited the best cytotoxic results relative to the standard. The CDK2 inhibition study revealed that compound **5** showed a prominent inhibitory effect (IC_{50} = 0.56 μM), superior to that of the reference drug, roscovitine (IC_{50} = 0.99 μM). Moreover, cell cycle analysis demonstrated that compound **5** induced cell arrest at both S phase and G2 phase compared with the control, in addition to its ability to trigger apoptosis, raise the Bax level, and reduce the Bcl-2 level in the MCF-7 cells. Finally, the process by which the synthesized pyrazole derivatives suppress the growth of cancer was examined by running CDK2 docking simulations.

Author contributions

Samar A. Abubshait: supervision, writing – original draft. Lamia H. T. Amin: investigation, methodology, writing – original draft. Abeer M. El-Naggar: data curation, supervision, writing – original draft. Mohamed G. Elbanna: methodology, writing – original draft. Kurls E. Anwer: investigation, methodology, data curation, formal analysis, writing, conceptualization, supervision, validation, writing – review & editing.

Conflicts of interest

All authors confirm that no competing personal, financial, and/or professional interests exist that may influence the work reported in this article.

Data availability

All data supporting the findings of this study are included in the article and its supplementary information (SI) files. Supplementary information: including FTIR, 1HNMR, 13CNMR, Rational, Cell cycle analysis, effects of compounds on apoptosis of MCF-7, and molecular docking studies. See DOI: **https://doi.org/10.1039/d5ra05212b**.

Acknowledgements

I would like to thank the Basic and Applied Scientific Research Centre at Imam Abdulrahman Bin Faisal University, KSA, for funding and supporting the analysis.

References

1 E. I. Edache, A. Adedayo, H. A. Dawi and F. A. Ugbe, Drug-like screening, molecular docking, molecular dynamics simulations, and binding free energies on the interaction of pyrazole derivatives as inhibitors of lysosomal storage disorders and anticancer activity, *Discov. Chem.*, 2024, **1**, 22–32, DOI: **10.1007/s44371-024-00025-7**.

2 E. A. Kurls, E. A. Nour, M. S. Marium, Y. Z. Mohamed and Y. B. Botros, Design, Green Synthesis and Tailoring of Vitamin E TPGS Augmented Niosomal Nano-Carrier of Pyrazolopyrimidines as Potential Anti-Liver and Breast Cancer Agents with Accentuated Oral Bioavailability, *Pharmaceuticals*, 2022, **15**, 330–368, DOI: **10.3390/ph15030330**.

3 A. A. Alsfouk, I. M. Othman, M. M. Anwar, W. A. Alshareef, A. Saleh and E. S. Nossier, Synthesis and computational studies of new pyridine, pyrazole, pyran, and pyranopyrimidine-based derivatives of potential antimicrobial activity as DNA gyrase and topoisomerase IV inhibitors, *J. Mol. Struct.*, 2025, **1319**, 139528–139548, DOI: **10.1016/j.molstruc.2024.139528**.

4 A. Z. Omar, S. I. Nabil, E. A. Hamed, H. Y. Alharbi, M. S. Aljohani and M. A. El-Atawy, Synthesis, characterization, and color performance of bis-azo and bis-pyrazole derivatives for dyeing of polyester, *J. Mol. Struct.*,

2025, **1322**, 140474–140485, DOI: 10.1016/j.molstruc.2024.140474.

5 M. Sofan, F. El-Taweel, A. Abdel-Rahman, H. Salman and E. Negm, Synthesis of novel azo pyrazole disperse dyes for dyeing and antibacterial finishing of PET fabric under supercritical carbon dioxide, *Sci. Rep.*, 2024, **14**, 1121–1133, DOI: 10.1038/s41598-023-48740-y.

6 A. Matine, B. Es-Sounni, M. Bakhouch, A. H. Bahkali, H. E. A. El Abdallaoui, S. Wang and A. Zeroual, Design, synthesis, and evaluation of a pyrazole-based corrosion inhibitor: a computational and experimental study, *Sci. Rep.*, 2024, **14**, 25238–25256, DOI: 10.1038/s41598-024-76300-5.

7 E. E. El-Katori, R. A. El-Saeed and M. M. Abdou, Anti-corrosion and anti-microbial evaluation of novel water-soluble bis azo pyrazole derivative for carbon steel pipelines in petroleum industries by experimental and theoretical studies, *Arab. J. Chem.*, 2022, **15**, 104373–104393, DOI: 10.1016/j.arabjc.2022.104373.

8 M. Alsulaimany, A. K. Aljohani, N. E. Abd El-Sattar, S. A. Almadani, O. M. Alatawi, H. Y. Alharbi and K. E. Anwer, Dual VEGFR-2 and EGFRT790M inhibitors of phenyldiazenes: anticancer evaluations, ADMET, docking, design and synthesis, *Future Med. Chem.*, 2025, **17**, 287–300, DOI: 10.1080/17568919.2025.2453409.

9 M. Alsulaimany, M. F. A. Abdulhaleem, R. Alghamdi, N. E. Abd El-Sattar, S. A. Almadani, W. A. Samman and K. E. Anwer, ADMET, docking, anticancer evaluations, design and synthesis of pyrazolo [1, 5-a] pyrimidines substituted with furan and phenyldiazene as dual EGFRT790M and VEGFR-2 inhibitors, *Bioorg. Chem.*, 2025, **163**, 108746, DOI: 10.1016/j.bioorg.2025.108746.

10 K. E. Anwer, B. Y. Beshay, M. M. Shamaa and N. E. Abd El-Sattar, Design and synthesis of pyrazolopyrimidinone derivatives as dual VEGFR/Aurora kinase inhibitors against hepatocellular and breast carcinomas, *Biomed. Pharmacother.*, 2025, **192**, 118679, DOI: 10.1016/j.biopha.2025.118679.

11 R. Kavitha, S. Prabhu, N. Prakash, S. Amalraj, M. Ayyanar, S. Kadaikunnan and J. M. Khaled, Design and synthesis of a novel pyrazole-based molecule with potential anticancer and antimicrobial effects: a multifaceted in silico approach, *J. Mol. Struct.*, 2025, **1323**, 140536–140552, DOI: 10.1016/j.molstruc.2024.140536.

12 O. Roby, F. Z. Kadiri, M. Moutaouakil, F. E. Z. Ousaid, R. Saddik, A. Aboulmouhajir and S. Tighadouini, Synthesis, characterization, DFT calculations, antimicrobial activity, molecular docking, and ADMET study of new pyrazole-carboxamide derivatives, *J. Mol. Struct.*, 2025, **1322**, 140400–140417, DOI: 10.1016/j.molstruc.2024.140400.

13 M. A. A. Reheim, H. S. A. Rady, O. A. Mohamed, A. Hassan, I. S. A. Hafiz, H. M. Reffat and A. H. Abdelmonsef, Synthesis, Anti-Inflammatory, and Molecular Docking Studies of New Heterocyclic Derivatives Comprising Pyrazole, Pyridine, and/or Pyran Moieties, *Pharmaceuticals*, 2025, **18**, 335–356, DOI: 10.3390/ph18030335.

14 V. M. Patil and H. N. More, Unlocking Anti-Inflammatory Potential: Virtual Discovery and ADMET Evaluation of Novel Pyrazole-Based COX-II Inhibitors, *Indian J. Pharm. Educ. Res.*, 2025, **59**, s312–s322, DOI: 10.5530/ijper.20256457.

15 M. N. Khadri, R. Ramu, N. A. Simha and S. A. Khanum, Synthesis, molecular docking, analgesic, anti-inflammatory, and ulcerogenic evaluation of thiophene-pyrazole candidates as COX, 5-LOX, and TNF-α inhibitors, *Inflammopharmacology*, 2024, **32**, 693–713, DOI: 10.1007/s10787-023-01364-0.

16 Y. Zhang, Z. Gao, J. Xu, B. Liu, P. Qin and M. Ji, Synthesis and acaricidal activity of novel pyrazole acrylonitrile derivatives, *Chin. J. Pestic. Sci.*, 2024, **26**, 716–723, DOI: 10.16801/j.issn.1008-7303.2024.0061.

17 A. Jyothsna and K. P. Latha, Pyrazole-quinazoline hybrids as potent antimicrobial and anthelmintic activity: design, synthesis, characterization, *World J. Pharm. Res.*, 2024, **13**, 1067–1080, DOI: 10.20959/wjpr20245-31564.

18 H. A. Siddiq, M. A. Imam, S. T. Alsharif, R. M. Attar, R. Almughathawi, N. M. Alshammari and N. M. El-Metwaly, Synthesis of New Thiazole-Pyrazole Analogues: Molecular Modelling, Antiproliferative/Antiviral Activities, and ADME Studies, *Chem. Biol. Drug Des.*, 2025, **105**, e70090–e70102, DOI: 10.1111/cbdd.70090.

19 X. Lei, J. Tan, P. Zhu, C. Zheng, Y. Liu, L. Zhang and J. Hu, Bidentate pyridine-pyrazole ligand-induced synergistic and antagonistic effects for selective separation of nickel from sulfuric acid medium, *Sep. Purif. Technol.*, 2025, **35**, 129188–129198, DOI: 10.1016/j.seppur.2024.129188.

20 L. M. Aroua, I. S. Alkhaibari, F. M. Alminderej, S. Messaoudi, S. Chigurupati, S. A. Al-mahmoud and H. A. Mohammed, Synthesis, bioactivity, and molecular docking of pyrazole bearing Schiff-bases as prospective dual alpha-amylase and alpha-glucosidase inhibitors with antioxidant activity, *J. Mol. Struct.*, 2025, **1320**, 139291–139303, DOI: 10.1016/j.molstruc.2024.139291.

21 O. Merzouki, N. Arrousse, E. Ech-chihbi, A. S. Alanazi, E. H. Mabrouk, M. Hefnawy and M. Taleb, Environmentally Friendly Synthesis of New Mono-and Bis-Pyrazole Derivatives; In Vitro Antimicrobial, Antifungal, and Antioxidant Activity; and In Silico Studies: DFT, ADMETox, and Molecular Docking, *Pharmaceuticals*, 2025, **18**, 167–203, DOI: 10.3390/ph18020167.

22 V. Kovač, T. Lukačević, D. Jadreško, J. Mrvčić, D. Stanzer, K. Hanousek-Čiča and I. Kmetič, Novel Ferrocene-Containing Pyrazole Analogs of Curcumin: Synthesis, Characterization, Antioxidant Activity, Cyclic Voltammetry, and In Vitro Biological Evaluation, *Appl. Organomet. Chem.*, 2025, **39**, e7753–e7768, DOI: 10.1002/aoc.7753.

23 W. Q. Yu, L. X. Zhao, Y. Bian, P. X. Zhang, L. Jia, D. M. Zhao and F. Ye, Pharmacophore Recombination Design, Synthesis, and Bioactivity of Ester-Substituted Pyrazole Purine Derivatives as Herbicide Safeners, *J. Agric. Food Chem.*, 2025, **73**, 3341–3352, DOI: 10.1021/acs.jafc.4c07027.

24 B. T. Abd-Elhalim, G. G. El-Bana, A. F. El-Sayed and G. E. Abdel-Ghani, Antifungal activity and biocompatibility

assessment with molecular docking and dynamic simulations of new pyrazole derivatives, *BMC Biotechnol.*, 2025, **25**, 15–36, DOI: 10.1186/s12896-025-00948-8.

25 O. Ommi, P. S. Dhopat, S. Sau, M. R. Estharla, S. Nanduri, N. P. Kalia and V. M. Yaddanapudi, Design, synthesis, and biological evaluation of pyrazole–ciprofloxacin hybrids as antibacterial and antibiofilm agents against Staphylococcus aureus, *RSC Med. Chem.*, 2025, **16**, 420–428, DOI: 10.1039/D4MD00623B.

26 K. Vashisht, P. Sethi, S. K. Ramasamy, A. Bansal, M. O. Dar, M. Singh and S. Baskoutas, Synthesis, characterization, and antibacterial activity of novel pyrazole derivatives, *J. Mol. Struct.*, 2025, **1332**, 141706–141718, DOI: 10.1016/j.molstruc.2025.141706.

27 E. M. Husseiny, R. M. Abdelnaby, N. Altwaijry, A. Saleh and K. E. Anwer, Comparison between conventional, grinding, and microwave synthesis of methylpyrazoles as VEGFR-2/HSP90 dual inhibitors, *Future Med. Chem.*, 2025, **17**, 899–913, DOI: 10.1080/17568919.2025.2485866.

28 E. M. El-Fawal, A. M. El Naggar, N. E. Abd El-Sattar and K. E. Anwer, CuZrO3@ Functionalized-organic matrix as a novel composite for enhanced photocatalytic treatment of antibiotics-contaminated wastewater, *Surf. Interfaces*, 2025, **68**, 106670–106688, DOI: 10.1016/j.surfin.2025.106670.

29 M. H. Ahmed, M. A. El-Hashash, M. I. Marzouk and A. M. El-Naggar, Synthesis and antitumor activity of some nitrogen heterocycles bearing pyrimidine moiety, *J. Heterocycl. Chem.*, 2020, **57**, 3412–34271, DOI: 10.1002/jhet.4061.

30 M. M. Mehany, O. A. Hammam, A. A. Selim, G. H. Sayed and K. E. Anwer, Novel pyridine bearing pentose moiety-based anticancer agents: design, synthesis, radioiodination and bioassessments, *Sci. Rep.*, 2024, **14**, 2738, DOI: 10.1038/s41598-024-53228-4.

31 R. Kamani, D. Raval, K. Patel, V. Prajapati, R. Prajapati, U. Shah and S. N. Mali, One-Pot multicomponent synthesis of novel pyrazole-linked thiazolyl-pyrazolines: molecular docking and cytotoxicity assessment on breast and lung cancer cell-lines, *J. Mol. Struct.*, 2025, **1322**, 140295, DOI: 10.1016/j.molstruc.2024.140295.

32 H. M. Naguib, N. T. Dauoud, S. N. Shaban, N. F. Abdelghaffar, G. H. Sayed and K. E. Anwer, Synthesis of Pyrazolone Derivatives by Grinding, Microwave, and Conventional Techniques and Their Antimicrobial Activity, *Russ. J. Org. Chem.*, 2022, **58**, 891–904, DOI: 10.1134/S1070428022060203.

33 K. E. Anwer, G. H. Sayed, A. Kozakiewicz-Piekarz and R. M. Ramadan, Novel annulated thiophene derivatives: synthesis, spectroscopic, X-ray, Hirshfeld surface analysis, DFT, biological, cytotoxic, and molecular docking studies, *J. Mol. Struct.*, 2022, **1276**, 134798–134816, DOI: 10.1016/j.molstruc.2022.134798.

34 A. M. El-Naggar, A. Khalil, H. Zeidan and W. M. El-Sayed, Eco-friendly Synthesis of Pyrido[2,3-d] pyrimidine Analogs and Their Anticancer and Tyrosine Kinase Inhibition Activities, *Anti-Cancer Agents Med. Chem.*, 2017, **17**, 1644–1651, DOI: 10.2174/1871521409666170412130040.

35 E. M. Husseiny, H. S. Abulkhair, N. M. El-Dydamony and K. E. Anwer, Exploring the cytotoxic effect and CDK-9 inhibition potential of novel sulfaguanidine-based azopyrazolidine-3,5-diones and 3,5-diaminoazopyrazoles, *Bioorg. Chem.*, 2023, **133**, 106397–106412, DOI: 10.1016/j.bioorg.2023.106397.

36 A. M. El-Naggar, M. M. Hemdan and S. R. Atta-Allah, An Efficient One-Pot Synthesis of New Coumarin Derivatives as Potent Anticancer Agents under Microwave Irradiation, *J. Heterocycl. Chem.*, 2017, **54**, 3519–3526, DOI: 10.1002/jhet.2975.

37 E. M. Abbass, A. K. Khalil and A. M. El-Naggar, Eco-friendly synthesis of novel pyrimidine derivatives as potential anticancer agents, *J. Heterocycl. Chem.*, 2020, **57**, 1154–1164, DOI: 10.1002/jhet.3852.

38 G. H. Sayed, M. E. Azab and K. E. Anwer, Conventional and microwave-assisted synthesis and biological activity study of novel heterocycles containing pyran moiety, *J. Heterocycl. Chem.*, 2019, **56**, 2121–2133, DOI: 10.1002/jhet.3606.

39 K. E. Anwer and G. H. Sayed, Conventional and microwave reactions of 1, 3-diaryl-5, 4-enaminonitrile-pyrazole derivative with expected antimicrobial and anticancer activities, *J. Heterocycl. Chem.*, 2020, **57**, 2339–2353, DOI: 10.1002/jhet.3946.

40 K. E. Anwer, S. S. El-Hddad, N. E. Abd El-Sattar, A. El-Morsy, F. Khedr, S. Mohamady and N. S. Hanafy, Five and six membered heterocyclic rings endowed with azobenzene as dual EGFR T790M and VEGFR-2 inhibitors: design, synthesis, in silico ADMET profile, molecular docking, dynamic simulation and anticancer evaluations, *RSC Adv.*, 2023, **13**, 35321–35338, DOI: 10.1039/d3ra06614b.

41 O. M. Elbakry, M. F. Harras, M. M. Elsebaei, A. Mehany and H. Elsehrawi, Development of pyrazolo [1, 5-a] pyrimidine derivatives: synthesis, anticancer activity and docking study, *Azhar International Journal of Pharmaceutical and Medical Sciences*, 2024, **4**, 76–90.

42 G. H. Sayed, N. A. Negm, M. E. Azab and K. E. Anwer, Synthesis, Characterization and Biological Activity of Some Pyrazole-Pyrazolone Derivatives, *Egypt. J. Chem.*, 2016, **59**, 663–672, DOI: 10.21608/ejchem.2016.1442.

43 D. J. Baillache and A. Unciti-Broceta, Recent developments in anticancer kinase inhibitors based on the pyrazolo [3, 4-d] pyrimidine scaffold, *RSC Med. Chem.*, 2020, **11**, 1112–1135, DOI: 10.1039/D0MD00227E.

44 M. Y. Zamanian, N. Taheri, M. F. Ramadan, Y. F. Mustafa, S. Alkhayyat, K. N. Sergeevna and S. Daneshvar, A comprehensive view on the fisetin impact on colorectal cancer in animal models: focusing on cellular and molecular mechanisms, *Anim. Models Exp. Med.*, 2024, **7**, 591–605, DOI: 10.1002/ame2.12476.

45 D. A. Patel, S. S. Patel and H. D. Patel, Advances in synthesis and biological evaluation of CDK2 inhibitors for cancer therapy, *Bioorg. Chem.*, 2024, **143**, 107045–107100, DOI: 10.1016/j.bioorg.2023.107045.

46 E. Z. Mohammed, W. R. Mahmoud, R. F. George, G. S. Hassan, F. A. Omar and H. H. Georgey, Synthesis, in

vitro anticancer activity and in silico studies of certain pyrazole-based derivatives as potential inhibitors of cyclin dependent kinases (CDKs), *Bioorg. Chem.*, 2021, **116**, 105347–105362, DOI: 10.1016/j.bioorg.2021.105347.

47 A. Arias-Gómez, A. Godoy and J. Portilla, Functional pyrazolo [1, 5-a] pyrimidines: Current approaches in synthetic transformations and uses as an antitumor scaffold, *Molecules*, 2021, **26**(9), 2708, DOI: 10.3390/molecules26092708.

48 J. C. Castillo and J. Portilla, Recent advances in the synthesis of new pyrazole derivatives, *Targets Heterocycl. Syst.*, 2018, **22**, 194–223, DOI: 10.17374/targets.2019.22.194.

49 M. Kaliszczak, H. Patel, S. H. B. Kroll, L. Carroll, G. Smith, S. Delaney and E. O. Aboagye, Development of a cyclin-dependent kinase inhibitor devoid of ABC transporter-dependent drug resistance, *Br. J. Cancer*, 2013, **109**, 2356–2367, DOI: 10.1038/bjc.2013.584.

50 A. S. Hassan, G. O. Moustafa, H. M. Awad, E. S. Nossier and M. F. Mady, Design, synthesis, anticancer evaluation, enzymatic assays, and a molecular modeling study of novel pyrazole–indole hybrids, *ACS Omega*, 2021, **6**, 12361–12374, DOI: 10.1021/acsomega.1c01604.

51 S. J. Almehmadi, A. M. Alsaedi, M. F. Harras and T. A. Farghaly, Synthesis of a new series of pyrazolo [1, 5-a] pyrimidines as CDK2 inhibitors and anti-leukemia, *Bioorg. Chem.*, 2021, **117**, 105431, DOI: 10.1016/j.bioorg.2021.105431.

52 J. Van Meerloo, G. J. Kaspers and J. Cloos, Cell sensitivity assays: the MTT assay, *Cancer cell culture: methods and protocols*, 2011, vol. 731, pp. 237–245, DOI: 10.1007/978-1-61779-080-5_20.

53 K. E. Anwer, G. H. Sayed and R. M. Ramadan, Synthesis, spectroscopic, DFT calculations, biological activities and molecular docking studies of new isoxazolone, pyrazolone, triazine, triazole and amide derivatives, *J. Mol. Struct.*, 2022, **1256**, 132513–132529, DOI: 10.1016/j.molstruc.2022.132513.

54 H. A. Bashmail, A. A. Alamoudi, A. Noorwali, G. A. Hegazy, G. AJabnoor, H. Choudhry and A. M. Al-Abd, Thymoquinone synergizes gemcitabine anti-breast cancer activity via modulating its apoptotic and autophagic activities, *Sci. Rep.*, 2018, **8**, 11674–11685, DOI: 10.1038/s41598-018-30046-z.

55 E. M. Husseiny, H. S. Abulkhair, S. A. El-Sebaey, M. M. Sayed and K. E. Anwer, In vivo evaluation of novel synthetic pyrazolones as CDK9 inhibitors with enhanced pharmacokinetic properties, *Future Med. Chem.*, 2024, **16**, 2487–2505, DOI: 10.1080/17568919.2024.2419363.

56 A. A. Alqarni, A. A. Alamoudi, R. M. Allam, G. M. Ajabnoor, S. M. Harakeh and A. M. Al-Abd, The influence of antioxidant dietary-derived polyphenolic combination on breast cancer: molecular study, *Biomed. Pharmacother.*, 2022, **149**, 112835–112847, DOI: 10.1016/j.biopha.2022.112835.

57 G. S. Hassan, H. H. Georgey, E. Z. Mohammed, R. F. George, W. R. Mahmoud and F. A. Omar, Mechanistic selectivity investigation and 2D-QSAR study of some new antiproliferative pyrazoles and pyrazolopyridines as potential CDK2 inhibitors, *Eur. J. Med. Chem.*, 2021, **218**, 113389–113412, DOI: 10.1016/j.ejmech.2021.113389.

58 S. R. Majeed, M. A. Amin, F. A. Attaby and A. A. Soliman, Palladium Complexes Based on 2-Hydrazinopyridine Ligand: Synthesis, Spectroscopic Studies, DFT Calculations, and Cytotoxicity, *Biointerface Res. Appl. Chem.*, 2021, **11**, 14316–14335, DOI: 10.33263/BRIAC116.1431614335.

59 K. Yang, H. Q. Li, M. Q. Hu, M. X. Ma, Y. Q. Gu, Q. Y. Yang and Z. F. Chen, Sm (III), Gd (III), and Eu (III) complexes with 8-hydroxyquinoline derivatives as potential anticancer agents via inhibiting cell proliferation, blocking cell cycle, and inducing apoptosis in NCI-H460 cells, *Drug Dev. Res.*, 2024, **85**, e22265–e22276, DOI: 10.1002/ddr.22265.

60 J. R. Anacona and M. Rincones, Tridentate hydrazone metal complexes derived from cephalexin and 2-hydrazinopyridine: synthesis, characterization and antibacterial activity, *Spectrochim. Acta, Part A*, 2015, **141**, 169–175, DOI: 10.1016/j.saa.2015.01.009.

61 T. Topal, Synthesis, X-ray, characterization and HSA and energy framework analysis of novel pyridine-hydrazone based ligand and its Co (II) complex biological activity prediction and experimental antibacterial properties, *Mol. Cryst. Liq. Cryst.*, 2022, **741**, 94–113, DOI: 10.1080/15421406.2022.2060617.

62 N. S. Chundawat, V. K. Singh, N. P. Chauhan, P. S. S. Puri and A. B. Puri, Synthesis, characterization, molecular docking study of graphene oxide catalyzed novel Schiff base and their antimicrobial activities, *J. Adv. Sci. Res.*, 2021, **12**, 267–275.

63 S. P. Melal and N. O. Mahmoodi, A review of synthetic methods of 1,2,4-triazolopyridines and their therapeutic properties, *Results Chem.*, 2023, **5**, 100782–100800, DOI: 10.1016/j.rechem.2023.100782.

64 A. Chopra, 99mTc-succinimidyl-6-hydrazinopyridine-3-carboxylate-interleukin 12, *Molecular Imaging and Contrast Agent Database (MICAD)*, 2010.

65 H. M. Naguib, N. T. Dauoud, S. N. Shaban, N. F. Abdelghaffar, G. H. Sayed and K. E. Anwer, Synthesis of pyrazolone derivatives by grinding, microwave, and conventional techniques and their antimicrobial activity, *Russ. J. Org. Chem.*, 2022, **58**, 891–904, DOI: 10.1134/S1070428022060203.

66 B. M. Essa, A. A. Selim, G. H. Sayed and K. E. Anwer, Conventional and microwave-assisted synthesis, anticancer evaluation, 99mTc-coupling and In vivo study of some novel pyrazolone derivatives, *Bioorg. Chem.*, 2022, **125**, 105846–105856, DOI: 10.1016/j.bioorg.2022.105846.

67 K. Anwer, G. Sayed, H. Hassanan and M. Azab, Conventional and microwave synthesis of some new pyridine derivatives and evaluation their antimicrobial and cytotoxic activities, *Egypt. J. Chem.*, 2019, **62**, 707–726, DOI: 10.21608/EJCHEM.2018.5115.1452.

68 M. M. Mehany, O. A. Hammam, S. S. Mohamed, G. H. Sayed and K. E. Anwer, Design, Green Synthesis, and Anticancer

Activity of Novel Nicotinonitrile Derivatives, *Russ. J. Org. Chem.*, 2024, **60**, 329–341, DOI: **10.1134/S1070428024020167**.

69 K. E. Anwer and G. H. Sayed, Design, Synthesis, Antimicrobial, Anticancer, and Molecular Docking of Novel Quinoline Derivatives, *Russ. J. Org. Chem.*, 2024, **60**, 956–969, DOI: **10.1134/S107042802405018X**.

70 K. E. Anwer, N. M. El-Dydamony, A. Saleh, N. Altwaijry and E. M. Husseiny, Comparative Study of Conventional, Grinding, and Microwave-Assisted Synthesis of Aminopyrazolones and Diaminopyrazoles: Exploring the Antitumor Activity, Dual CDK-2/CA IX Inhibition Potential, and Apoptosis, *Drug Dev. Res.*, 2025, **86**, e70139–e70141, DOI: **10.1002/ddr.70139.0**.

71 K. E. Anwer, G. H. Sayed, B. M. Essa and A. A. Selim, Green synthesis of highly functionalized heterocyclic bearing pyrazole moiety for cancer-targeted chemo/radioisotope therapy, *BMC Chem.*, 2023, **17**, 139–150, DOI: **10.1186/s13065-023-01053-7**.

72 A. Kamal, B. Shaik, V. L. Nayak, B. Nagaraju, J. S. Kapure, M. S. Malik and B. Prasad, Synthesis and biological evaluation of 1, 2, 3-triazole linked aminocombretastatin conjugates as mitochondrial mediated apoptosis inducers, *Bioorg. Med. Chem.*, 2014, **22**, 5155–5167, DOI: **10.1016/j.bmc.2014.08.008**.

73 C. Fan, H. Su, J. Zhao, B. Zhao, S. Zhang and J. Miao, A novel copper complex of salicylaldehyde pyrazole hydrazone induces apoptosis through up-regulating integrin β4 in H322 lung carcinoma cells, *Eur. J. Med. Chem.*, 2010, **45**, 1438–1446, DOI: **10.1016/j.ejmech.2009.12.048**.

74 M. Saddam, S. K. Paul, M. A. Habib, M. A. Fahim, A. Mimi, S. Islam and M. M. U. Helal, Emerging biomarkers and potential therapeutics of the BCL-2 protein family: the apoptotic and anti-apoptotic context, *Egypt. J. Med. Hum. Genet.*, 2024, **25**, 12–40, DOI: **10.1186/s43042-024-00485-7**.

75 A. Cahyadi, I. D. G. Ugrasena, M. R. Andarsini, M. C. S. Larasati, A. Aryati and D. K. Arumsari, Relationship between Bax and Bcl-2 protein expression and outcome of induction phase chemotherapy in pediatric acute lymphoblastic leukemia, *Asian Pac. J. Cancer Prev.*, 2022, **23**, 1679–1685, DOI: **10.31557/APJCP.2022.23.5.1679**.

76 W. F. De Azevedo, S. Leclerc, L. Meijer, L. Havlicek, M. Strnad and S. H. Kim, Inhibition of cyclin-dependent kinases by purine analogues: crystal structure of human cdk2 complexed with roscovitine, *Eur. J. Biochem.*, 1997, **243**, 518–526, DOI: **10.1111/j.1432-1033.1997.0518a.x**.

77 A. Elengoe, C. H. Tan and S. Poddar, Computational analysis of antimicrobial phytochemicals from Bambusa vulgaris Schrad. ex JC Wendl.: pharmacokinetics, toxicity, and molecular docking, *Adv. Bamboo Sci.*, 2025, **11**, 100157–100169, DOI: **10.1016/j.bamboo.2025.100157**.

78 S. Chtita, S. Belaidi, F. A. Qais, M. Ouassaf, M. M. AlMogren, A. A. Al-Zahrani and T. Lakhlifi, Unsymmetrical aromatic disulfides as SARS-CoV-2 Mpro inhibitors: Molecular docking, molecular dynamics, and ADME scoring investigations, *J. King Saud Univ. Sci.*, 2022, **34**, 102226–102236, DOI: **10.1016/j.jksus.2022.102226**.

79 A. Daina, O. Michielin and V. Zoete, SwissADME: a free web tool to evaluate pharmacokinetics, drug-likeness and medicinal chemistry friendliness of small molecules, *Sci. Rep.*, 2017, **7**, 42717–42730, DOI: **10.1038/srep42717**.